Automatic Lung Segmentation for Accurate Quantitation of Volumetric X-Ray CT Images

Shiying Hu, Eric A. Hoffman, *Member, IEEE*, and Joseph M. Reinhardt*, *Member, IEEE*

***Abstract*—Segmentation of pulmonary X-ray computed tomography (CT) images is a precursor to most pulmonary image analysis applications. This paper presents a fully automatic method for identifying the lungs in three-dimensional (3-D) pulmonary X-ray CT images. The method has three main steps. First, the lung region is extracted from the CT images by gray-level thresholding. Then, the left and right lungs are separated by identifying the anterior and posterior junctions by dynamic programming. Finally, a sequence of morphological operations is used to smooth the irregular boundary along the mediastinum in order to obtain results consistent with those obtained by manual analysis, in which only the most central pulmonary arteries are excluded from the lung region.**

The method has been tested by processing 3-D CT data sets from eight normal subjects, each imaged three times at biweekly intervals with lungs at 90% vital capacity. We present results by comparing our automatic method to manually traced borders from two image analysts. Averaged over all volumes, the root mean square difference between the computer and human analysis is 0.8 pixels (0.54 mm). The mean intrasubject change in tissue content over the three scans was 2.75% ± 2.29% (mean ± standard deviation).

***Index Terms*—Image segmentation, pulmonary imaging, volumetric imaging, X-ray CT.**

I. Introduction

HIGH-RESOLUTION X-ray computed tomography (CT) is the standard for pulmonary imaging. Depending on the scanner hardware, CT can provide high spatial and high temporal resolution, excellent contrast resolution for the pulmonary structures and surrounding anatomy, and the ability to gather a complete three-dimensional (3-D) volume of the human thorax in a single breath hold [1]. Pulmonary CT images have been used for applications such as lung parenchyma density analysis [2], [3], airway analysis [4], [5], and lung and diaphragm mechanics analysis [6], [7]. A precursor to all of these quantitative analysis applications is lung segmentation. With the introduction of multislice spiral CT scanners, the number of volumetric studies of the lung is increasing and it is critical to develop fast, accurate algorithms that require minimal to no human interaction to identify the precise boundaries of the lung.

A number of groups have developed techniques for computer-assisted segmentation of pulmonary CT images [2], [8]–[14]. In [10], manually traced boundaries were used to estimate regional gas and tissue volumes in the lungs of normal subjects. But manual methods are laborious and subject to both interobserver and intraobserver variations. On two-dimensional (2-D) transverse slices of a pulmonary CT dataset, the natural contrast between the low-density lungs and the surrounding high-density chest wall can be used to guide image segmentation. In [2], [8], and [9], 2-D edge tracking was used to find the boundaries of the left and right lungs. Others have used 3-D region growing with manually specified seed points [2], [12]–[14]. In many semi-automatic approaches, some manual interaction is required to select threshold values or edit the resulting segmentation [2], [8], [9], [12]–[14]. In [8], anterior and posterior junction lines are provided manually to separate the right and left lungs in the case where the edge contrast is reduced by the volume averaging. More recently, Brown *et al.* [11] provided a knowledge-based, automatic method to segment chest CT images. In their method, anatomic knowledge stored in a semantic network is used to guide low-level image processing routines. Rather than requiring manual intervention to define the anterior junction lines as in [8], Brown *et al.* used dynamic programming to search for the junction lines automatically.

In this paper, we describe a fully automatic method for identifying the lungs in CT images. The method has three main steps. First, the lung region is extracted from the CT images by gray-level thresholding. The left and right lungs are then separated by detecting the anterior and posterior junctions. Finally, we optionally smooth the lung boundary along the mediastinum. There are several distinctions between our method and previous work. First, instead of using a fixed threshold value, we use an optimal thresholding method [15] to automatically choose a threshold value that reflects the gray-scale characteristics of a specific dataset. Second, we use an efficient method to find the anterior and posterior junction lines between the right and left lungs. Finally, to obtain more consistent results across time and to leave lung structures with the lung, we optionally smooth the irregular boundary along the mediastinum. We present results comparing our automatic method to manually traced borders from two image analysts. We have compared the automatic method to the manual analysis for a total of 12 3-D volumes. Averaged over all volumes, the root mean square (rms) difference between the computer and human analysis is about 0.8 pixels (corresponding to about 0.54 mm). By studying the same subject repeatedly over a short time interval (1–2 weeks), we are

Manuscript received June 30, 2000; revised March 20, 2001. This work was supported in part by a Biomedical Engineering Research Grant from the Whitaker Foundation and by the National Institutes of Health (NIH) under Grant HL64368-01 and Grant HL60158-02. The Associate Editor responsible for coordinating the review of this paper and recommending its publication was A. Manduca. *Asterisk indicates corresponding author.*

S. Hu is with the Department of Biomedical Engineering, University of Iowa, Iowa City, IA 52242 USA.

E. A. Hoffman is with the Department of Radiology, University of Iowa, Iowa City, IA 52242 USA.

*J. M. Reinhardt is with the Department of Biomedical Engineering, University of Iowa, Iowa City, IA 52242 USA (e-mail: joe-reinhardt@uiowa.edu).

Publisher Item Identifier S 0278-0062(01)04688-2.

able to demonstrate a consistent quantitative assessment of lung tissue content.

This paper is organized as follows. Section II gives a detailed description of the method. Section III provides experimental results, and Section IV contains a discussion and summary.

II. Methods

We assume that the input data is a 3-D X-ray CT data set organized as a stack of 2-D transverse slices. For precise edge localization for quantitation, thin (1–2 mm or thinner) contiguous slices will yield the best results. If possible, the data set should include the thorax from the trachea to below the diaphragm. In the CT image data, air will appear with a mean intensity of approximately -1000 Hounsfield units (HU), most lung tissue will be in the range of -910 HU to -500 HU, while the chest wall, blood, and bone will be much more dense (well above -500 HU) [11], [16]. As discussed in [14], HU can be converted to percent air content for a more meaningful link to known lung morphometry.

As shown in Fig. 1, our method consists of three main steps: an extraction step to identify the lungs; a separation step to separate the right and left lungs; and an optional smoothing step to smooth the lung boundaries. Each of these steps is described in detail next.

A. Lung Extraction

The goal of the lung extraction step is to separate the voxels corresponding to lung tissue from the voxels corresponding to the surrounding anatomy. Rather than using a fixed threshold to segment the lungs, we instead use optimal thresholding [15] to automatically select a segmentation threshold for the image volume. Connectivity and topological analysis are used to further refine regions that represent the extracted lungs.

1) Threshold Selection: Optimal thresholding is an automatic threshold selection method that allows us to accommodate the small variations in tissue density expected across a population of subjects. For this step, we assume that the image volume contains only two types of voxels: 1) voxels within the very dense body and chest wall structures (the *body* voxels) and 2) low-density voxels in the lungs or in the air surrounding the body of the subject (the *nonbody* voxels). We will use optimal thresholding to select a segmentation threshold to separate the body from the nonbody voxels, and then identify the lungs as the low-density cavities inside of the body.

The segmentation threshold is selected through an iterative procedure. Let T^i be the segmentation threshold at step i. To choose a new segmentation threshold, we apply T^i to the image to separate the voxels into body and nonbody voxels. Let μ_b and μ_n be the mean gray-level of the body voxels and nonbody voxels after segmentation with threshold T^i. Then the new threshold for step $i+1$ is

$$T^{i+1} = \frac{\mu_b + \mu_n}{2}.$$

This iterative threshold update procedure is repeated until there is no change in the threshold, i.e., $T^{i+1} = T^i$. The initial threshold T^0 is selected based on the CT number for pure air

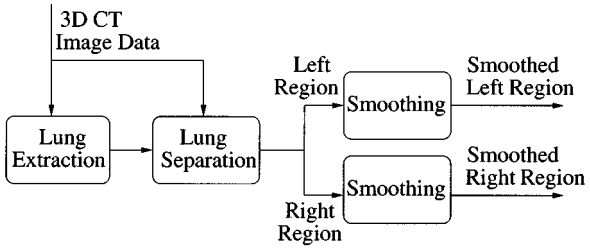

Fig. 1. Lung segmentation method diagram.

(-1000 HU) and the CT number for voxels within the chest wall/body (>0 HU).

2) Connectivity and Topological Analysis: After applying the optimal threshold, the nonbody voxels will correspond to the air surrounding the body, the lungs, and other low-density regions within the image volume (i.e., gas in the bowel). Three-Dimensional connected components labeling is used to identify the lung voxels. The background air is eliminated by deleting regions that are connected to the border of the image. Small, disconnected regions are discarded if the region volume is too small. To identify the lungs, we retain the only the two largest components in the volume, with the additional constraint that each component must be larger than a predetermined minimum volume. In this paper, we retain only the components with a volume greater than one percent of the total image voxel count.

The high-density vessels in the lung will be labeled as body voxels during the optimal thresholding step. As a result, the 3-D lung regions will contain unwanted interior cavities. Topological analysis, similar to that used in [17], is used to fill the lung regions and eliminate the interior cavities.

3) Segmentation of the Large Airways: To perform quantitative analyses on the lung tissue, the trachea and large airways must be identified and separated from the left and right lungs. This step is also necessary to facilitate the left and right lung separation described in Section II-B

The trachea and left and right mainstem bronchi are identified in the original gray-level image data using a closed-space dilation with a unit radius kernel [18]. This procedure is equivalent to directed slice-by-slice region growing. To initialize the closed-spaced dilation, the location of the trachea is automatically identified by searching for the large, circular, air-filled region near the center of the first few slices in the data set. Regions in the current slice provide potential seed point positions for the next slice. The slice-by-slice growing procedure is stopped when the size of the region on a new slice increases dramatically, indicating that the airways have merged into the low-density lung tissue.

After the closed-space dilation, the original gray-scale image has been segmented into three regions: 1) the lungs; 2) the trachea and left and right mainstem bronchi; and 3) other regions. While the lung regions have been extracted, the left and right lungs have not yet been separately identified.

B. Left and Right Lung Separation

When viewed on transverse CT slices, the anterior and posterior junctions between the left and right lungs may be very thin with weak contrast [e.g., see Fig. 2(a) and (d)]. In many cases,

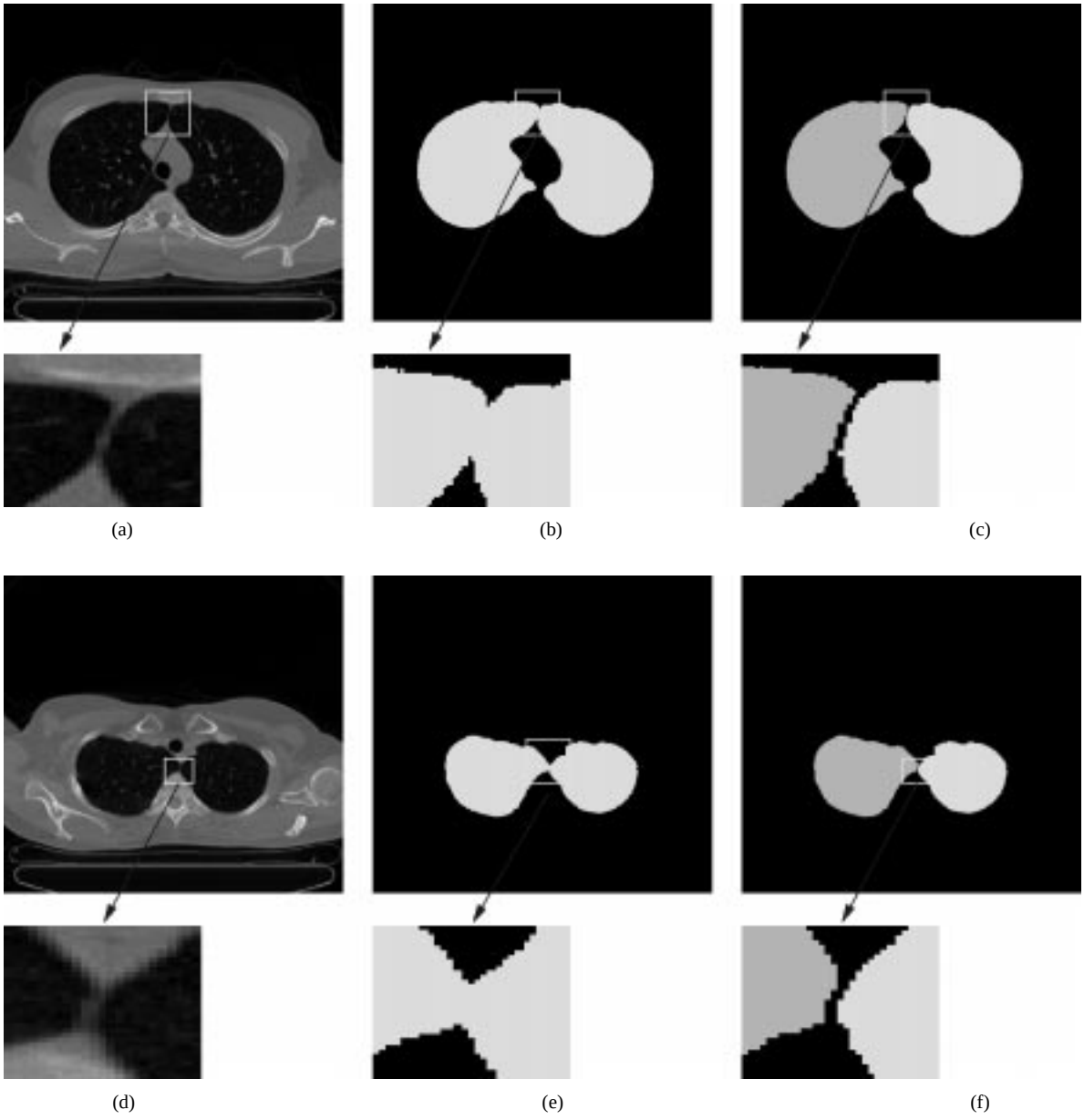

Fig. 2. (a), (d) Transverse CT slices from two healthy subjects. (a) Approximately 2.4 cm above carina. (d) Approximately 3.6 cm above carina. (b) and (e) show results after the initial lung segmentation. The left and right lungs are connected. (c) and (f) show results after two lungs are separated.

gray-scale thresholding fails to separate the left and right lungs near these junctions [see Fig. 2(b) and (e)] [8], [11]. The goal of the lung separation step is to locate these junction lines and completely separate the right and left lungs. Using a technique similar to that employed in [11], dynamic programming is applied to find the maximum cost path through a graph with weights proportional to pixel gray-level. The maximum cost path corresponds to the junction line position. However, we use a different strategy to find the dynamic programming search regions. In our method, a search region is found on a 2-D slice and it is propagated to successive slices. Because of the smooth pulmonary anatomy, the junction line position varies slowly through the data set. By avoiding the 3-D morphology operation used in [11], computation time is reduced. To further reduce computation time, we only apply the lung separation step to those slices that contain a single, large, connected lung component.

To find the region for applying the dynamic programming search on one slice, 2-D morphological erosion is applied to separate the right and left lungs. A conditional dilation is then used to restore the approximate original boundary shape, without reconnecting the two lungs again. Let A represent the set of lung pixels on a single slice. To separate the left and right lungs we compute a new set S using an n-fold erosion

$$S = A \ominus nB_4$$

where $\ominus$ is a binary morphological erosion and B_4 is a four-connected (diamond-shaped) binary structuring element. The scaling term n is selected so that nB_4 is the smallest homothetic that results in A and S having a different number of 2-D connected components.

After separating the lungs by erosion to form S, the boundary is restored using a conditional dilation. The conditional dilation

proceeds iteratively. The result of the conditional dilation at step $i+1$ is

$$C^{i+1} = C^i \cup \{\{p\} \oplus B_4\} \tag{1}$$

where $\oplus$ is a binary morphological dilation and $p \in C^i \cap A$, with the selection of p further constrained so that C^i and C^{i+1} have the same number of 2-D connected components. $C^0 = S$ is used to initialize the conditional dilation. This formulation guarantees that the lung boundary is recovered without rejoining the left and right lung halves. The conditional dilation in (1) is repeated until no pixels $p \in C^i \cap A$ are left that can be added without changing the connectivity of the regions in C^i.

Let C represent the result after conditional dilation. While the left and right lungs have been separated at this point, the separation was accomplished using region shape properties (via the morphological operators) without including the gray-scale characteristics of the anterior and posterior junction lines. Since the junction lines are slightly brighter than the surrounding lung tissue, gray-scale information can be used to more accurately define the separation between the two lungs.

To identify the anterior and posterior junction lines, we examine the difference between the lung regions before and after separation, $A \backslash C$. If $A \backslash C$ is nonempty, the pixels in $A \backslash C$ define the search region for the dynamic programming junction search [11]. Unlike [11], however, our approach allows us to identify both the anterior and posterior junction lines. Fig. 2(c) and (f) shows the results after detecting the anterior junction line and posterior junction line for a typical data set.

C. Smoothing

In [8], [10], manual editing was used to obtain satisfactory lung region borders after gray-scale processing. In our method, gray-scale thresholding followed by the topological processing and the lung separation step is sufficient to obtain good results without manual intervention. However, we include one additional optional smoothing step that can improve the overall results.

The lung regions near the mediastinum contain the radiodense pulmonary arteries and veins. By the gray-level processing described above, these vessels may be excluded from the lung regions [see Fig. 3(a) and (b)]. But when manually tracing the lung contours, a manual analyst may "cut" across the large pulmonary vessels and group them with the lung regions [see Fig. 3(c)], yielding a smooth lung contour. A similar situation occurs as the mainstem bronchi merge into the lungs. Gray-scale thresholding may include these large airways with the lung regions because of volume averaging ([see Fig. 4(a) and (b)]. Some manual analysts trace lung borders around the airways [see Fig. 4(d)], while others trace across them [see Fig. 4(c)]. Unfortunately, there is no well-defined standard criterion that specifies how define the lung boundary along the mediastinum, and for many cases the most appropriate segmentation will depend on the specific application.

We include an optional lung boundary shape smoothing step to give a smoothed lung boundary that more closely mimics the borders defined by some manual analysts. The smoothing step uses operations from binary mathematical morphology to address three shape-related issues: boundary indentations caused by the large pulmonary vessels; large boundary bulges caused by the left and right mainstem bronchi merging into the lungs; and small boundary bulges caused by small airways near the lung borders. In the description that follows, we describe the smoothing operations that are applied to the left and right lungs separately.

1) Pulmonary Vessels: A morphological closing is used to fill the indentations on the lung border caused by the pulmonary vessels. Let L represent the set of lung regions pixel on a 2-D slice. The smoothed region L^1 is computed by $L^1 = L \bullet R_f B_4$, where $\bullet$ is a binary morphological closing and R_f is a size parameter that determines what size vessels will be eliminated during smoothing.

2) Small Airways: To remove the small airways, an operation similar to a morphological opening is used. We first separate the airways from the lungs by an erosion, then we use connected components analysis to identify the largest component (corresponding to the lung). After identifying the largest component, a dilation is used to restore the approximate original border shape. For a set L of lung region pixels on a 2-D slice, this sequence of operations is used to remove the small airways

$$\begin{aligned} L^1 &= L \ominus R_{sa} B_4 \\ L^2 &= \text{conncomp}(L^1, 1) \\ L^3 &= L^2 \oplus R_{sa} B_4 \end{aligned}$$

where R_{sa} is a size parameter that controls the small airway shape smoothing and conncomp$(A, 1)$ returns the largest component of the set A.

3) Large Airways: To remove the big airways, again we use an operation similar to a morphological opening. However, in this case a large structuring element is usually required to detach the large airways from the lung regions, so the opening operation alone may cause too much shape deformation. To preserve the boundary details, we use the following procedure.

Similar to the sequence of steps used to remove the small airways, an erosion is first applied to the original binary regions L to separate the lungs from the big airways. Connected components analysis is used to identify the lung region. Next, the difference between the original region L and the smoothed region is computed. This difference contains the big pieces that correspond to the big airways, plus some small pieces that correspond to boundary details. We use connected components analysis to identify the big airways in the difference image. Finally, we compute the difference between the original region L and the difference image with the big airways. As a result, we are able to delete the large airways while preserving the boundary details. The entire sequence of steps is as follows:

$$\begin{aligned} L^1 &= L \ominus R_{ba} B_4 \\ L^2 &= \text{conncomp}(L^1, 1) \\ L^3 &= L^2 \oplus R_{ba} B_4 \\ L^4 &= L \setminus L^3 \\ L^5 &= \text{compsize}(L^4, v) \\ L^6 &= L \setminus L^5 \end{aligned}$$

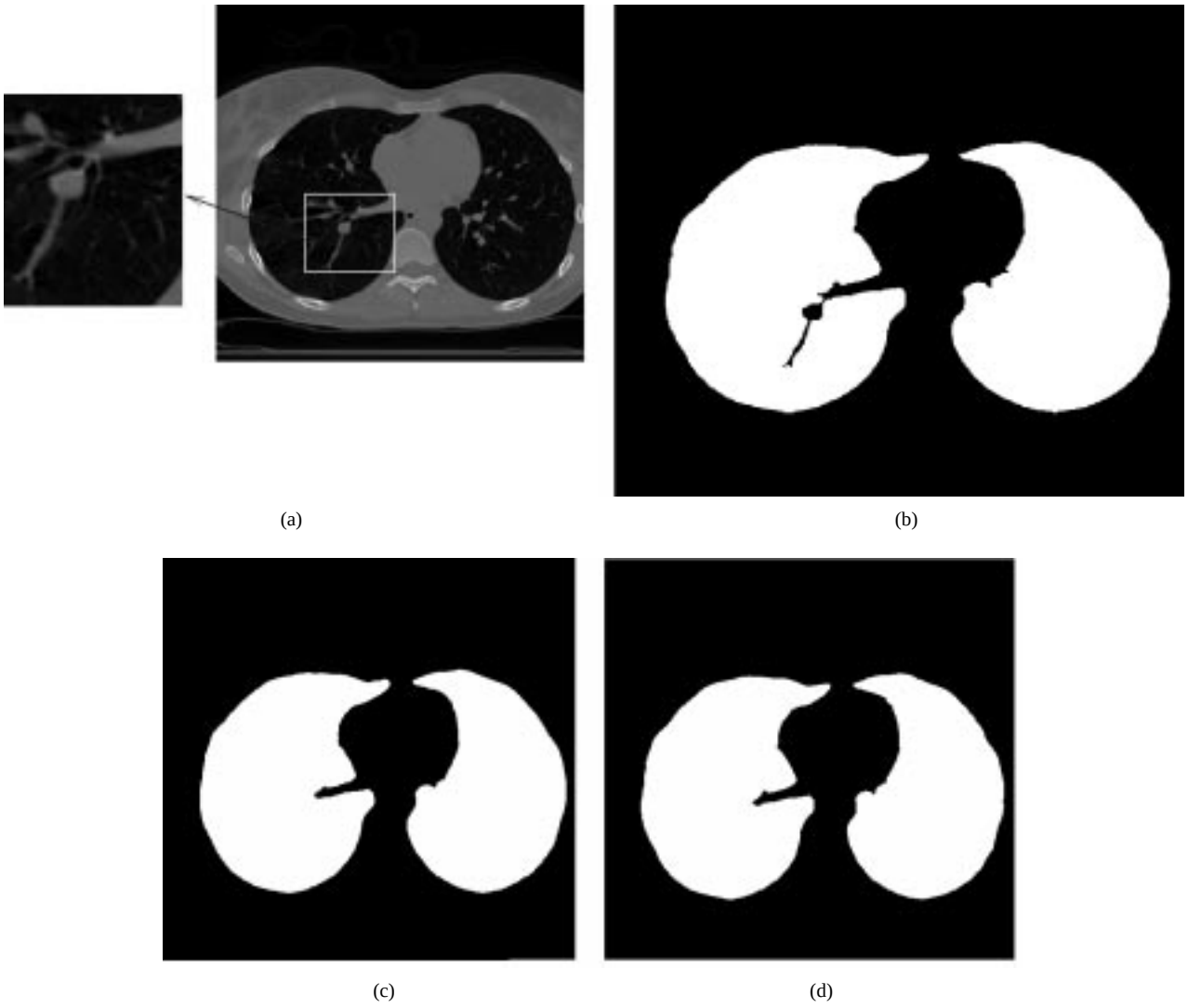

Fig. 3. (a) Transverse CT slice from a normal subject. (b) Segmentation result without smoothing. (c) Manual tracing result. (d) Automatic results after smoothing with $R_{sa} = 3$, $R_{ba} = 8$, and $R_f = 2$.

where compsize(A, v) returns all components in A that contain at least v pixels. In this paper, we use $v = 300$ pixels.

4) Selection of Shape-Smoothing Parameters: The three shape-smoothing parameters, R_f, R_{sa}, and R_{ba}, can be adjusted to control the behavior of the boundary smoothing step. Different smoothing effects to mimic different manual tracing behaviors can be obtained by varying R_f, R_{sa}, and R_{ba}. For example, if R_{sa} and R_{ba} are set to zero, both the large and small airways near the lung boundaries will be untouched, while the pulmonary vessels will be smoothed based on the parameter R_f.

Fig. 3(d) illustrates the effect of smoothing the borders near the pulmonary vessels with the parameter R_f. Fig. 4(e) and (f) shows two different smoothing results obtained by varying R_{sa} and R_{ba}. This figure shows that the two results closely mimic the two different manual tracing styles at the inner boundaries, but retain the shape information at outer boundaries. For the results presented in Section III, smoothing parameters $R_f = 2$, $R_{sa} = 3$, and $R_{ba} = 8$ were used. These parameters were found to give results close to those provided by two manual analysts (see Section III).

5) Shape-Smoothing Region: The shape smoothing is applied to the left and right lungs separately, to avoid reconnecting them near the anterior and posterior junctions. To reduce computation time and avoid undesired shape alterations to regions of the lung boundary not affected by the pulmonary vessels or airways merging into the lungs, we limit the shape smoothing to a small region near the mediastinum, as determined by the locations of the left and right mainstem bronchi.

III. Results

The algorithm was evaluated using 24 3-D CT datasets from eight normal subjects. Each subject was scanned three times, at approximately two week intervals. All scans were performed with the subject at full inspiration (90% vital capacity) with air volume monitored using a lung volume control method incorporated into a commercial pulmonary function monitoring system (Vmax, Sensor-Medics, Yorba Linda, CA) [19]. The images were acquired on an electron-beam CT scanner (EBCT) (Imatron C-150L, Imatron Inc., South San Francisco, CA). For each scan, a stack of 100–120 3-mm thin, contiguous slices covering

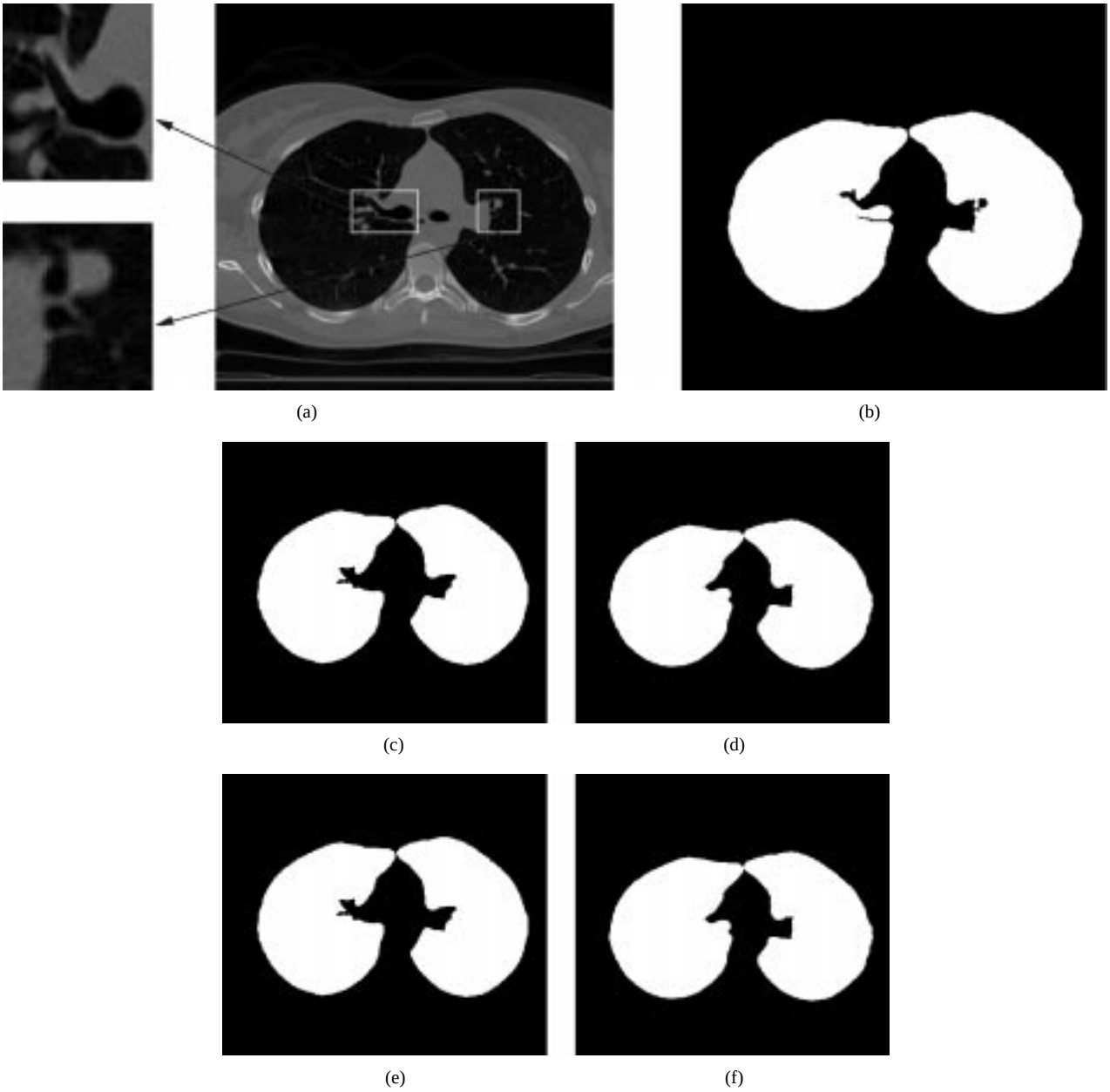

Fig. 4. (a) Transverse CT slice from a normal subject. (b) Segmentation result without smoothing. (c), (d) Manual tracing results from two different analysts. (e) Automatic results after smoothing with $R_{sa} = 0$, $R_{ba} = 0$, and $R_f = 2$. (f) Automatic results after smoothing with $R_{sa} = 3$, $R_{ba} = 8$, and $R_f = 2$.

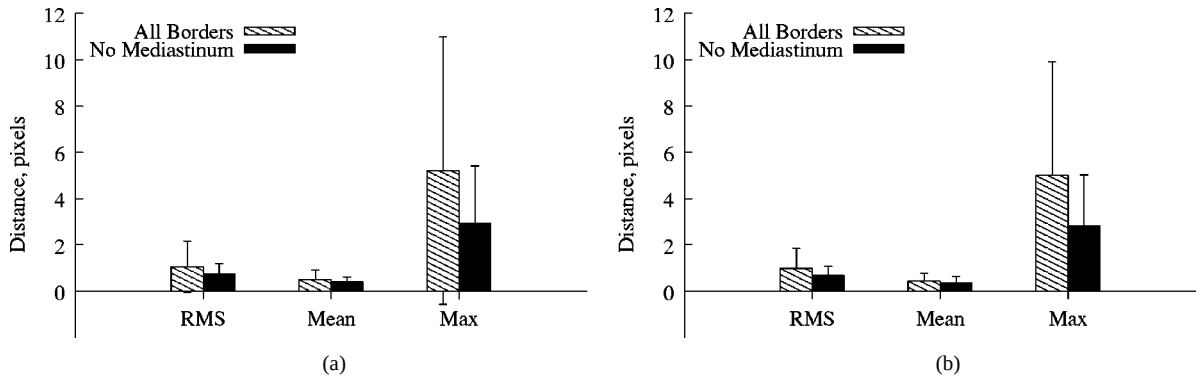

Fig. 5. Border positioning accuracy as assessed by distance measures from (3)–(5). (a) Automatic method versus Observer 1. (b) Automatic method versus Observer 2. Figures include mean, rms, and maximum distance averaged over 229 2D slices. Figures show results using all pixels on the border (indicated by "All Borders") and those using all pixels except those adjacent to the mediastinum (indicated by "No Mediastinum").

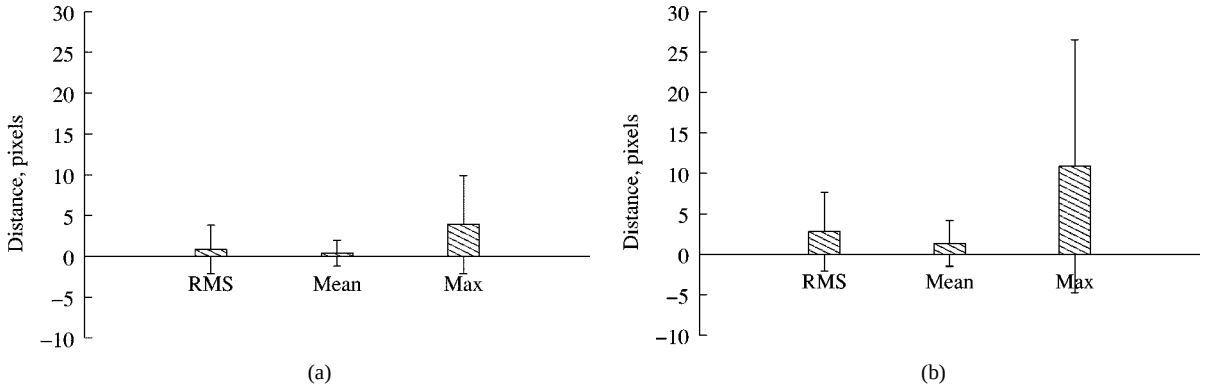

Fig. 6. Border positioning accuracy as assessed by distance measures from (3)–(5). (a) Observer 1 versus Observer 2. (b) Observer 2 versus Observer 1. Figures include mean, rms, and maximum distance averaged over all traced borders.

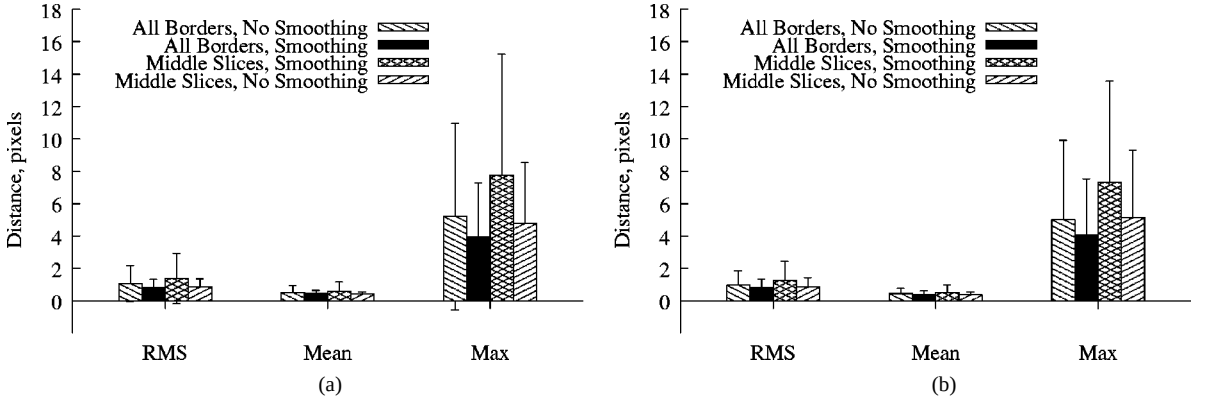

Fig. 7. Border positioning accuracy as assessed by distance measures from (3)–(5). (a) Automatic method versus Observer 1. (b) Automatic method versus Observer 2. Figures include mean, rms, and maximum distance averaged over entire borders (indicated by "All Borders, No Smoothing" and "All Borders, Smoothing"), and averaged over borders in middle slices (indicated by "Middle Slices, No Smoothing" and "Middle Slices, Smoothing").

the lungs were acquired. The EBCT scan aperture was 100 ms, with the scanner running in continuous volume imaging mode. The reconstruction field-of-view ranged from 30 to 35 cm, with a normal reconstruction kernel. Pixel sizes ranged from 0.586 to 0.684 mm.

A. Comparison with Manual Analysis

Segmentation accuracy was assessed by comparing the automatic computer-based segmentation with results obtained by manual analysis. Two image analysts manually traced the left and right lung borders on every fifth slice for 12 of the image data sets. Overall, each analyst traced the left and right lung borders on 229 slices. The analysts worked independently of each other and both analysts used the same software system to perform the analysis [20]. One analyst was very experienced (over six years of experience), while the other analyst had approximately one year of image analysis experience. While neither of the analysts were radiologists, both work closely with radiologists and are familiar with their requirements and expectations.

Border positioning accuracy was assessed by computing the mean, rms, and maximum distance between the computer-defined borders and the manually defined borders. For each pixel on the computer-defined borders, the minimum distance to the manually defined border was computed as

$$d_i = \min_j \left\{ \sqrt{(x_i^A - x_j^M)^2 + (y_i^A - y_j^M)^2} \right\} \tag{2}$$

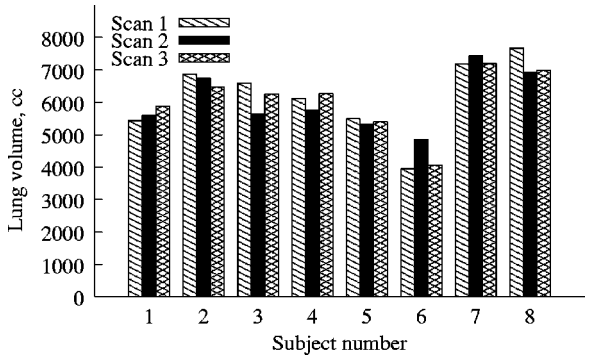

Fig. 8. Reproducibility as assessed by lung volume measurement. Subjects were scanned three times at approximately two-week intervals.

where (x_i^A, y_i^A) is the computer-defined border pixel location and (x_j^M, y_j^M) is a manually defined border pixel location [21]. For each computer-defined border, the mean, rms, and maximum distance to the manually traced border were computed using (3)–(5)

$$d_{\text{mean}} = \frac{\sum_{i=1}^{l} d_i}{l} \tag{3}$$

$$d_{\text{rms}} = \sqrt{\frac{\sum_{i=1}^{l} d_i^2}{l}} \tag{4}$$

$$d_{\max} = \max_i d_i \tag{5}$$

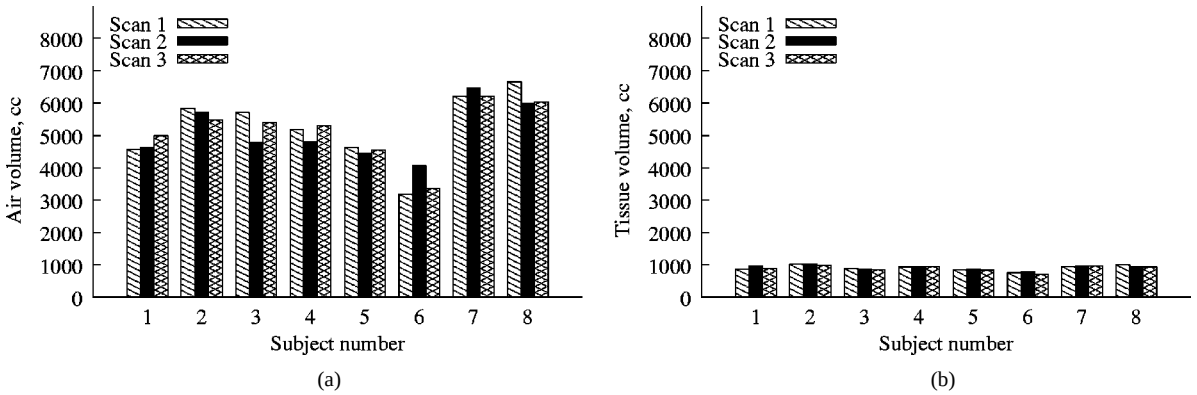

Fig. 9. Lung volume decomposed into air volume and tissue volume. (a) Air volume. (b) Tissue volume. As expected, tissue volume remains relatively constant while air volume changes because subjects have difficulty returning to the exactly same volume for each scan.

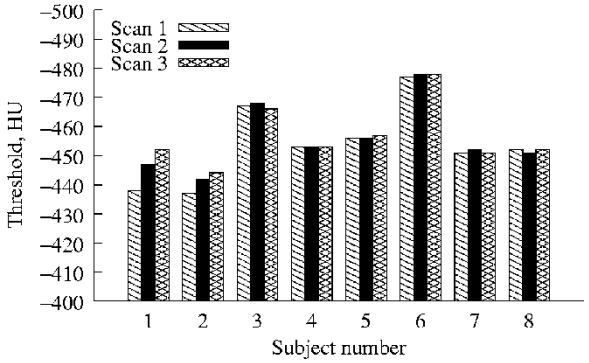

Fig. 10. Automatically selected segmentation threshold across three repeated scans.

where l is the number of points on the computer-defined borders. Unless otherwise noted, the following results present statistics computed over all 229 manually traced slices.

Fig. 5 shows a comparison between the manually identified borders and the computer-defined borders. The figure shows the difference between observer 1 and the computer, and the difference between observer 2 and the computer. The results are similar for both of these cases. The figure shows the rms error computed over all boundary pixels, and the rms error if we exclude pixels near the mediastinum. The figure shows that the greatest difference between computer-defined borders and manually defined borders occur on the borders near the mediastinum.

For comparison, we also evaluated the interobserver variations by computing the distances between the borders defined by the manual analysts. These results are shown in Fig. 6.

Fig. 7 shows the effect of applying the optional shape smoothing step with our selected parameters $R_f = 2$, $R_{sa} = 3$, and $R_{ba} = 8$. These figures show the mean, rms, and maximum distance between the computer-defined and manually defined borders computed over the entire lung and over a limited number of slices near the mediastinum. From the results, it is clear that the smoothing step improves the accuracy, especially for the boundaries near the mediastinum.

B. Reproducibility and Calculation of Lung Volumes

The repeat scans of the same subjects were used to assess method reproducibility. For each subject, the three scans were analyzed and used to compute left and right lung volumes. Lung volumes were computed by taking the product of the number of voxels in the segmented lungs and the voxel dimensions. These results are shown in Fig. 8.

To understand the volume variations depicted in Fig. 8, the contributions of air volume and tissue volume were computed separately for each scan. For each voxel, the fractional air volume was computed using the method described in [14]. The remaining volume fraction of the voxel has been considered tissue (note that it actually consists of tissue, blood, and extra-vascular fluid). Fig. 9 shows the air volume and tissue volume for each subject across all three scans. The range of variation of intrasubject tissue volume measurement was 0.9%–7.0%, with a mean variation of $2.75\% \pm 2.29\%$ (mean $\pm$ standard deviation). Note that the greatest variation in intrasubject volume measurement is due to differences in air content, which are probably because of variability in the effort-dependent method for holding lung volume at a fixed level during scanning.

C. Automatic Threshold Selection

Optimal thresholding is used to calculate the gray-scale segmentation threshold for each data set. Fig. 10 shows how the automatically selected threshold varies across the three repeated scans.

IV. Discussion

CT lung density is influenced by factors such as subject tissue volume, air volume, image acquisition protocol, physical material properties of the lung parenchyma, and transpulmonary pressure. These factors make the selection of a gray-level segmentation threshold difficult, as different thresholds are likely required for different subjects. In earlier works, a single pre-determined threshold was used to separate the lungs from the surrounding anatomy [2], [8]–[10]. In our method, optimal thresholding is used to select a threshold value based on the unique characteristics of the data set. As shown in Fig. 10, there is little variation in the threshold across repeated scans of the same subject, while there is some minor variation across subjects. Optimal thresholding is also expected to perform better across variations in lung volume, where there are significant changes in lung density.

The comparison with manual analysis (Figs. 5 and 7) shows that when averaged over all pixels making up the

computer-defined lung boundary, the mean distance between the computer-defined borders and manually defined borders is about 0.48 pixels. When the border regions near the mediastinum are eliminated from the calculation, the mean distance drops to about 0.37 pixels. The optional smoothing step reduces the mean distance to about 0.41 pixels. The smoothing step reduces the border curvature near the mediastinum, more closely matching the borders manually defined by the image analysts. For comparison, the mean distance between the borders defined by the two manual analysts (Fig. 6) is about 0.88 pixels. Thus, the mean distance between the computer and either of the observers is smaller than the mean distance between the two observers alone.

Lung volume computed from the segmented images shows that the results are reproducible across time. The small variations in the computed lung volumes (Fig. 8) are primarily due to differences in the level of lung inflation, as the air volume varies while the tissue volume remains relatively constant (Fig. 9). This is due to the fact that lung volume level was defined as a percent of vital capacity, and the assessment of vital capacity (difference between full expiration and full inspiration) is effort dependent.

This method was tested on a PC workstation with 300-MHz processor and 512-MB RAM. On average, 2–3 min are required to segment a $512 \times 512 \times 120$ data set, plus an additional 1–2 min for the optional smoothing step.

ACKNOWLEDGMENT

The authors wish to thank J. Cook-Granroth and D. Chon for performing the manual image analysis.

REFERENCES

[1] E. A. Hoffman and G. McLennan, "Assessment of the pulmonary structure-function relationship and clinical outcomes measures: Quantitative volumetric CT of the lung," *Academic Radiol.*, vol. 4, no. 11, pp. 758–776, 1997.

[2] L. W. Hedlund, R. F. Anderson, P. L. Goulding, J. W. Beck, E. L. Effmann, and C. E. Putman, "Two methods for isolating the lung area of a CT scan for density information," *Radiology*, vol. 144, pp. 353–357, 1982.

[3] R. Uppaluri, T. Mitsa, M. Sonka, E. A. Hoffman, and G. McLennan, "Quantification of pulmonary emphysema from lung CT images using texture analysis," *Amer. J. Resp. Crit. Care Med.*, vol. 156, no. 1, pp. 248–254, 1997.

[4] I. Amirav, S. S. Kramer, M. M. Grunstein, and E. A. Hoffman, "Assessment of methacholine-induced airway constriction by ultrafast high-resolution computed tomography," *J. Appl. Physiol.*, vol. 75, no. 5, pp. 2239–2250, 1993.

[5] R. H. Brown, C. J. Herold, C. A. Hirshman, E. A. Zerhouni, and W. Mitzner, "In vivo measurement of airway reactivity using high resolution computed tomography," *Amer. Rev. Resp. Dis.*, vol. 144, no. 1, pp. 208–212, 1991.

[6] E. A. Hoffman, T. Behrenbeck, P. A. Chevalier, and E. H. Wood, "Estimation of regional pleural surface expansile forces in intact dogs," *J. Appl. Physiol.*, vol. 55, no. 3, pp. 935–948, 1983.

[7] A. M. Boriek, S. Liu, and J. R. Rodarte, "Costal diaphragm curvature in the dog," *J. Appl. Physiol.*, vol. 75, no. 2, pp. 527–533, 1993.

[8] W. A. Kalender, H. Fichte, W. Bautz, and M. Skalej, "Semiautomatic evaluation procedures for quantitative CT of the lung," *J. Comput. Assist. Tomogr.*, vol. 15, no. 2, pp. 248–255, 1991.

[9] J. M. Keller, F. M. Edwards, and R. Rundle, "Automatic outlining of regions on CT scans," *J. Comput. Assist. Tomogr.*, vol. 5, no. 2, pp. 240–245, 1981.

[10] D. M. Denison, M. D. L. Morgan, and A. B. Millar, "Estimation of regional gas and tissue volumes of the lung in supine man using computed tomography," *Thorax*, vol. 41, pp. 620–628, 1986.

[11] M. S. Brown, M. F. McNitt-Gray, N. J. Mankovich, J. G. Goldin, J. Hiller, L. S. Wilson, and D. R. Aberle, "Method for segmenting chest CT image data using an anatomical model: Preliminary results," *IEEE Trans. Med. Imag.*, vol. 16, pp. 828–839, Dec. 1997.

[12] E. A. Hoffman and E. L. Ritman, "Effect of body orientation on regional lung expansion in dog and sloth," *J. Appl. Physiol.*, vol. 59, no. 2, pp. 481–491, 1985.

[13] E. A. Hoffman, L. J. Sinak, R. A. Robb, and E. L. Ritman, "Noninvasive quantitative imaging of shape and volume of lungs," *J. Appl. Physiol. (Resp., Environ., Exercise Physiol.)*, vol. 54, no. 5, pp. 1414–1421, 1983.

[14] E. A. Hoffman, "Effect of body orientation on regional lung expansion: A computed tomographic approach," *J. Appl. Physiol.*, vol. 59, no. 2, pp. 468–480, 1985.

[15] M. Sonka, V. Hlavac, and R. Boyle, *Image Processing, Analysis and Machine Vision*. Pacific Grove, CA: PWS, 1999.

[16] M. Wu, J. Chang, A. A. Chiang, J. Lu, H. Hsu, W. Hsu, and C. Yang, "Use of quantitative CT to predict postoperative lung function in patients with lung cancer," *Radiology*, vol. 191, pp. 257–262, 1994.

[17] J. M. Reinhardt and W. E. Higgins, "Paradigm for shape-based image analysis," *Opt. Eng.*, vol. 37, no. 2, pp. 570–581, Feb 1998.

[18] Y. Masutani, K. Masamune, and T. Dohi, "Region-growing based feature extraction algorithm for tree-like objects," in *Lecture Notes in Computer Science*, K. H. Höhne and R. Kikinis, Eds. Berlin, Germany: Springer-Verlag, 1996, vol. 1131, pp. 161–171.

[19] B. Q. Tran, J. K. Tajik, R. A. Chiplunkar, and E. A. Hoffman, "Lung volume control for quantitative X-ray CT," *Ann. Biomed. Eng.*, vol. 24, no. 1, p. S-66, Oct 1996.

[20] E. A. Hoffman, D. Gnanaprakasam, K. B. Gupta, J. D. Hoford, S. D. Kugelmass, and R. S. Kulawiec, "VIDA: An environment for multidimensional image display and analysis," in *SPIE Conf. Biomedical Image Processing and Three -Dimensional Microscopy*, vol. 1660, 1992, pp. 1–18.

[21] V. Chalana and Y. Kim, "A methodology for evaluation of boundary detection algorithms on medical images," *IEEE Trans. Med. Imag.*, vol. 16, pp. 642–652, Oct. 1997.